

Supplementary Materials for

Microfluidics-based super-resolution microscopy enables nanoscopic characterization of blood stem cell rolling

Karmen AbuZineh, Luay I. Joudeh, Bader Al Alwan, Samir M. Hamdan,
Jasmeen S. Merzaban, Satoshi Habuchi*

*Corresponding author. Email: satoshi.habuchi@kaust.edu.sa

Published 18 July 2018, *Sci. Adv.* 4, eaat5304 (2018)
DOI: 10.1126/sciadv.aat5304

The PDF file includes:

- Fig. S1. The multistep paradigm of cell migration highlighting the main interactions that take place between the blood stem cell in flow and the endothelial cells lining the blood vessels of the bone marrow.
- Fig. S2. Surface density of E-selectin on the protein A–deposited microfluidic chamber determined by immunofluorescence imaging.
- Fig. S3. Flow cytometric analysis to determine the binding specificity of ligand-specific antibodies to CD44 on KG1a cells.
- Fig. S4. Localization precisions of the SR localization microscopy experiments of CD44 on KG1a cells.
- Fig. S5. Examples of the reconstructed SR images of CD44 on KG1a cells.
- Fig. S6. SR images of CD44 on KG1a cells.
- Fig. S7. Cluster analysis of the nanoscale architecture of lipid rafts on KG1a cells.
- Fig. S8. Examples of the reconstructed SR images of CD44 on M β CD-treated KG1a cells.
- Fig. S9. Cluster analysis of the nanoscale architecture of CD44 on KG1a cells.
- Fig. S10. Expression of CD44 on untreated and M β CD-treated KG1a cells was determined by flow cytometry.
- Fig. S11. Depth of the field in the SR localization microscopy imaging experiments with HILO configuration.
- Legends for movies S1 to S8

Other Supplementary Material for this manuscript includes the following:

(available at advances.sciencemag.org/cgi/content/full/4/7/eaat5304/DC1)

Movie S1 (.mp4 format). Time-lapse transmitted light microscopy images of KG1a cells perfused into the microfluidic chamber at the shear stress of 0.25 dyne cm⁻².

Movie S2 (.mp4 format). Time-lapse transmitted light microscopy images of KG1a cells perfused into the microfluidic chamber at the shear stress of 0.5 dyne cm^{-2} .

Movie S3 (.mp4 format). Time-lapse transmitted light microscopy images of KG1a cells perfused into the microfluidic chamber at the shear stress of 1.0 dyne cm^{-2} .

Movie S4 (.mp4 format). Time-lapse transmitted light microscopy images of KG1a cells perfused into the microfluidic chamber at the shear stress of 2.0 dyne cm^{-2} .

Movie S5 (.mp4 format). Time-lapse transmitted light microscopy images of KG1a cells perfused into the microfluidic chamber at the shear stress of 4.0 dyne cm^{-2} .

Movie S6 (.mp4 format). Time-lapse transmitted light microscopy images of KG1a cells perfused into the microfluidic chamber in the presence of EDTA (10 mM) at the shear stress of 1.0 dyne cm^{-2} .

Movie S7 (.mp4 format). Time-lapse transmitted light microscopy images of KG1a cells perfused into the microfluidic chamber at the shear stress of 1.0 dyne cm^{-2} .

Movie S8 (.mp4 format). Time-lapse transmitted light microscopy images of M β CD-treated KG1a cells perfused into the microfluidic chamber at the shear stress of 1.0 dyne cm^{-2} .

Supplementary Figures

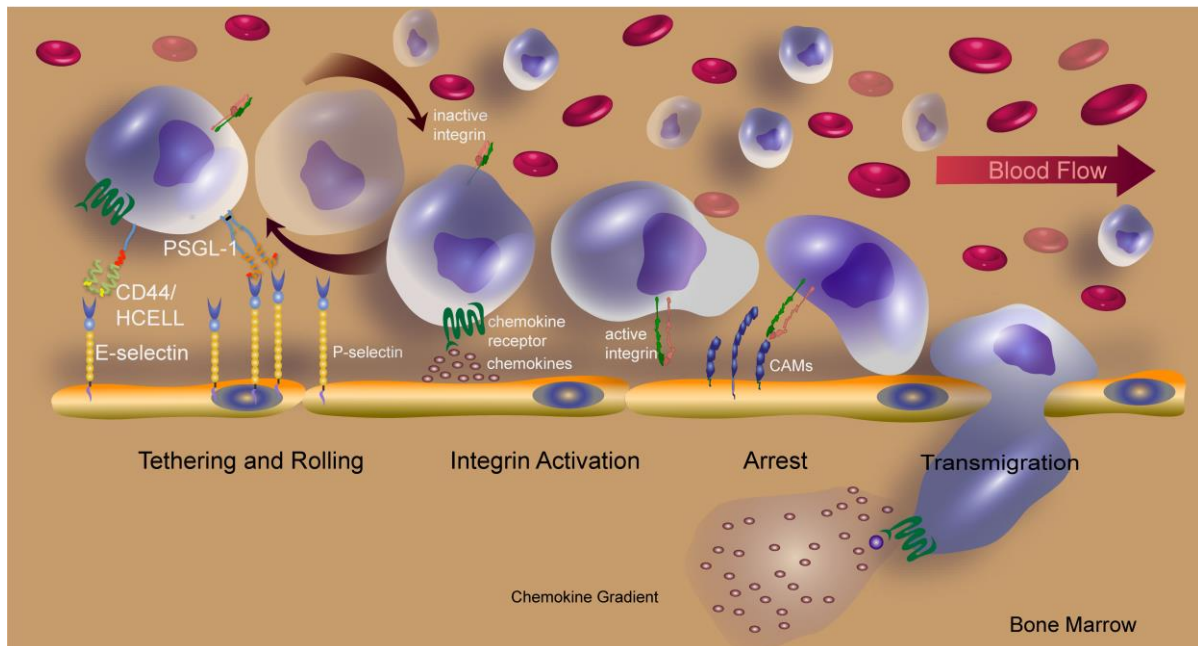


Fig. S1. The multistep paradigm of cell migration highlighting the main interactions that take place between the blood stem cell in flow and the endothelial cells lining the blood vessels of the bone marrow. Step 1, “tethering and rolling”, is mediated by the selectins (E- and P-selectin) and their ligands (CD44/HCELL and PSGL-1) and acts to slow down the cell. Step 2, “integrin activation” is controlled by chemokines on the surface of the endothelial cells and their appropriate chemokine receptors on the surface of the stem cell; this triggers G-protein-coupled “inside-out” activation of integrins. This activation results in conformational changes in the integrin(s) expressed on the stem cell in flow which results in high affinity binding of the integrin(s) to their CAM (cellular adhesion molecules) ligand(s) on the endothelium leading to Step 3 “firm adhesion”. The interaction of all of these molecules with their appropriate receptors culminates at Step 4, the transmigration of the stem cell into the bone marrow. Each step is a prerequisite for the next and the initial step is crucial in starting it all. O-glycans are shown as yellow squiggly lines and N-glycans are shown as green circles.

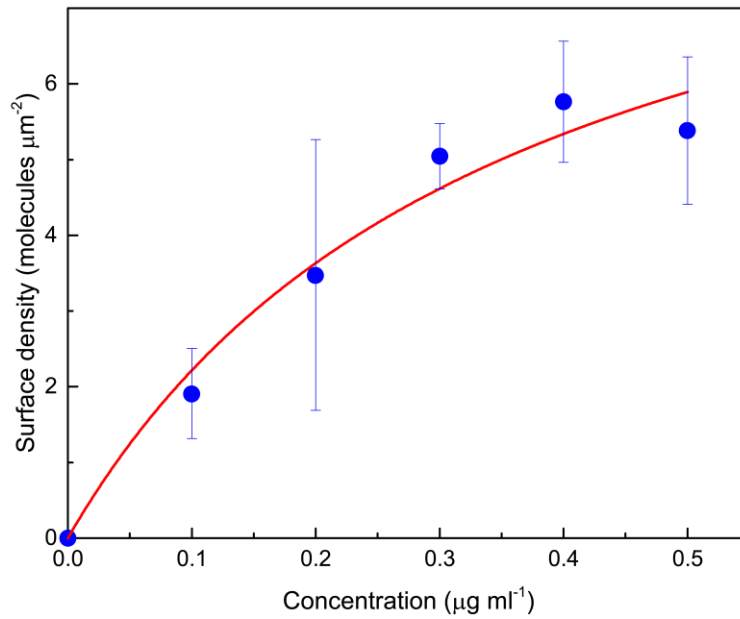


Fig. S2. Surface density of E-selectin on the protein A–deposited microfluidic chamber determined by immunofluorescence imaging. The surface densities are plotted against the concentration of E-selectin in the solution. The red line shows the fitting of the data with Langmuir adsorption model, where the surface density (Q) is described by the concentration of the molecule in the solution ($[C]$) and the adsorption constant (K_{ad}), $Q \propto K_{ad} \cdot [C]/(1 + K_{ad} \cdot [C])$. The error bars represent standard deviation of five independent experiments.

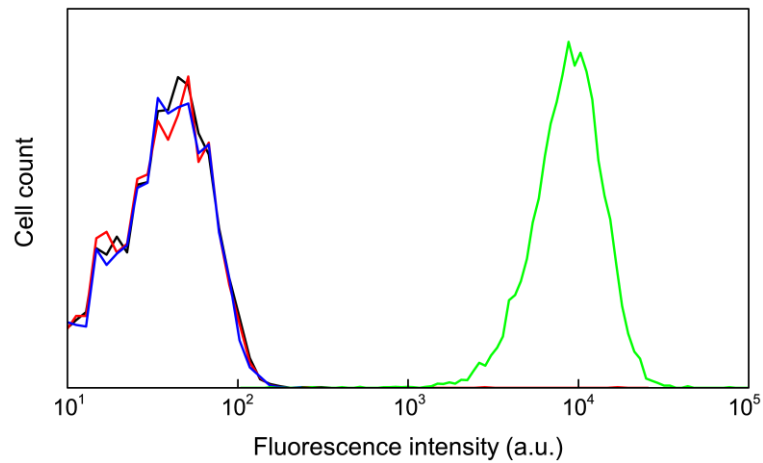


Fig. S3. Flow cytometric analysis to determine the binding specificity of ligand-specific antibodies to CD44 on KG1a cells. KG1a cells were labelled with CD44 antibodies (515) and AF-488-conjugated secondary antibodies against the CD44 antibodies (goat anti-mouse IgG, green). Unstained KG1a cells (black), isotype control labelled cells (red), and secondary alone-labelled cells (blue) were added as controls. The data confirmed the binding specificity of the CD44 antibodies to CD44 on KG1a cells.

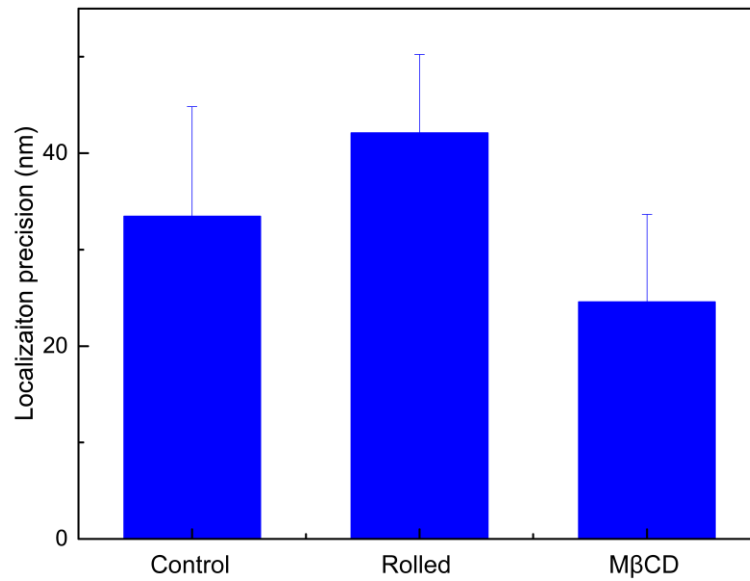


Fig. S4. Localization precisions of the SR localization microscopy experiments of CD44 on KG1a cells. Localization precisions were determined for KG1a cells that had either rolled over E-selectin or not (control) as well as for methyl- β -cyclodextrin (M β CD)-treated KG1a cells. Slight differences in the localization precision observed in each cell sample was mainly attributed to different background fluorescence from out-of-plane molecules in each cell sample.

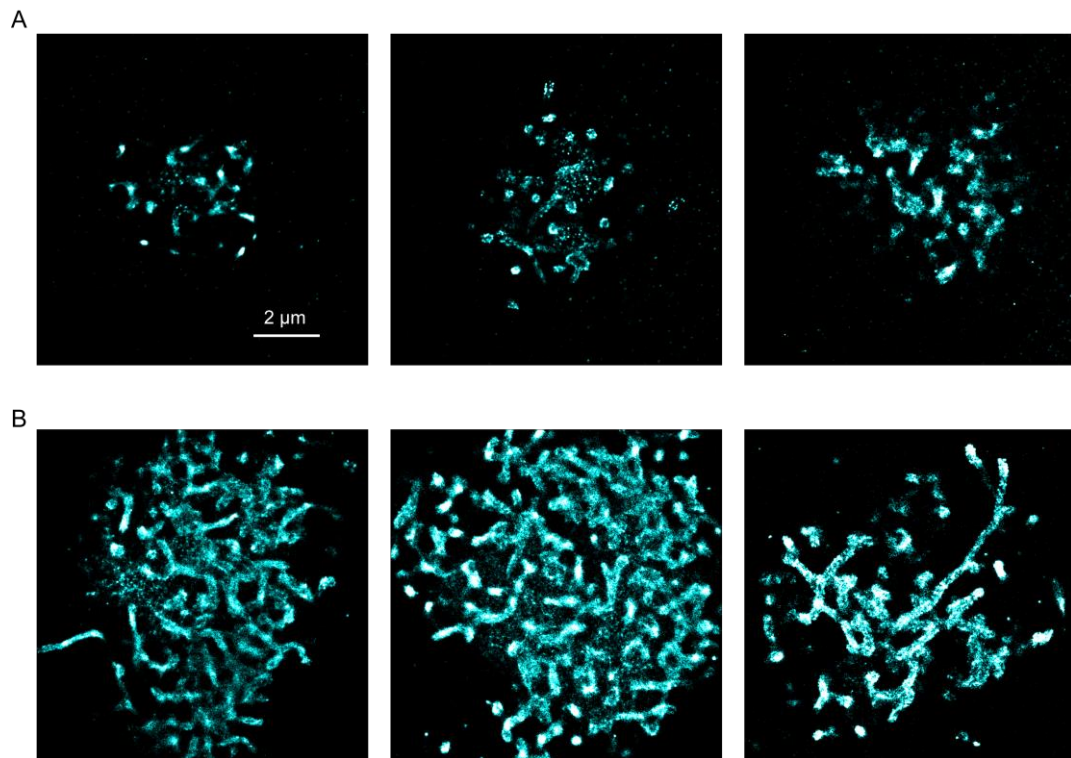


Fig. S5. Examples of the reconstructed SR images of CD44 on KG1a cells. KG1a cells either in suspension (**A**) or in the fluidic chamber after the rolling of the cells on E-selectin (**B**) were fixed and immunolabelled for CD44 using the 515 antibody followed by AF-647-conjugated secondary antibodies.

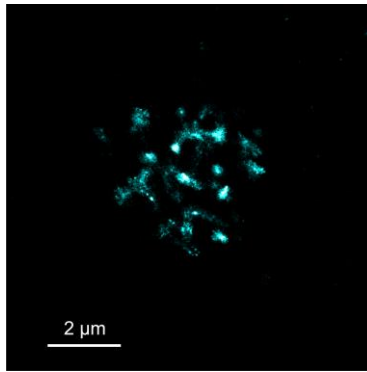


Fig. S6. SR images of CD44 on KG1a cells. KG1a cells in suspension were incubated with recombinant human E-selectin and fixed and immunolabeled for CD44 using the 515 antibody followed by AF-647-conjugated secondary antibodies.

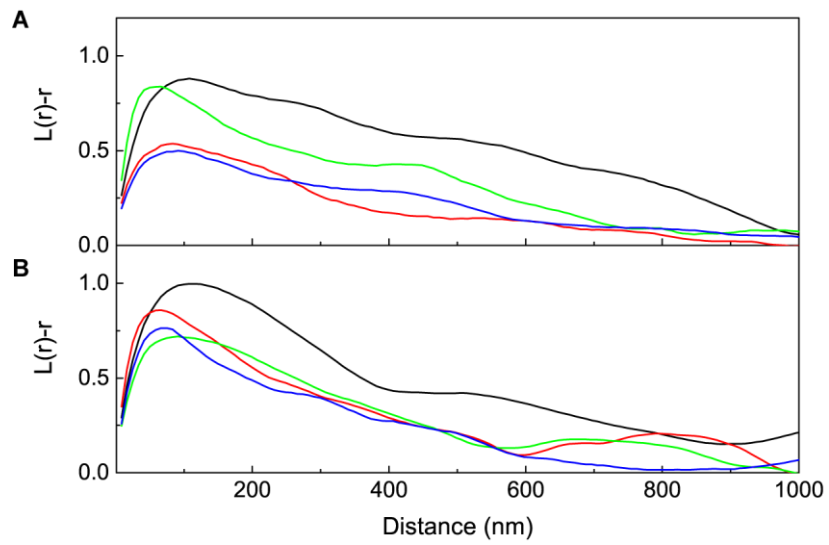


Fig. S7. Cluster analysis of the nanoscale architecture of lipid rafts on KG1a cells.

Examples of Ripley's K functions obtained from the super-resolution reconstructed images of lipid rafts on the (A) control KG1a cells and (B) rolled KG1a cells on E-selectins.

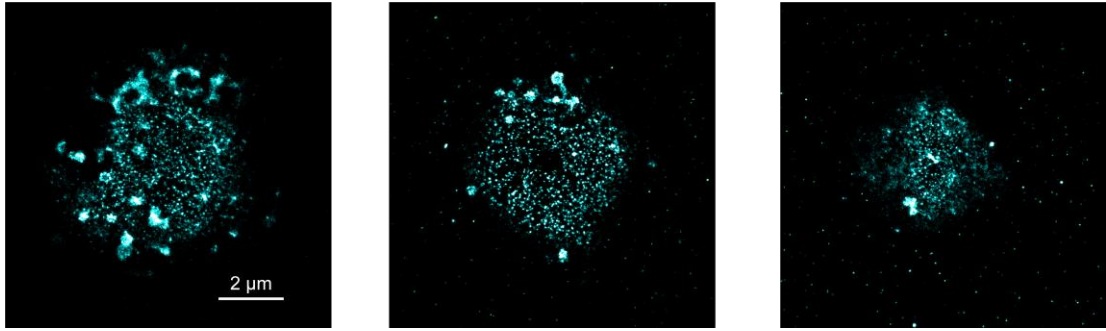


Fig. S8. Examples of the reconstructed SR images of CD44 on MβCD-treated KG1a cells. MβCD-treated KG1a cells in suspension were fixed and immunolabelled for CD44 using the 515 antibody followed by AF-647-conjugated secondary antibodies.

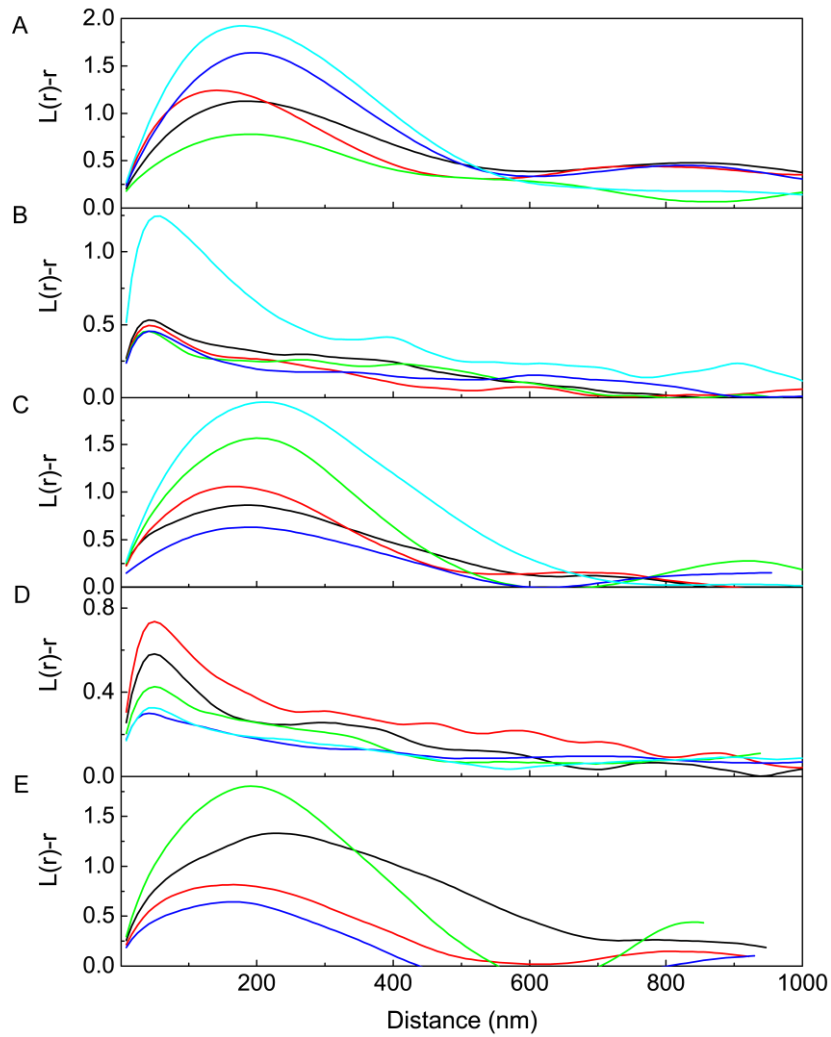


Fig. S9. Cluster analysis of the nanoscale architecture of CD44 on KG1a cells. Examples of Ripley's K functions obtained from the super-resolution reconstructed images of (A) CD44 on the control cells, (B) small clusters of CD44 on the M β CD-treated cells, (C) large clusters of CD44 on the M β CD-treated cells, (D) small clusters of CD44 on the M β CD-treated cells after rolling over E-selectins, and (E) large clusters of CD44 on the M β CD-treated cells after rolling over E-selectins.

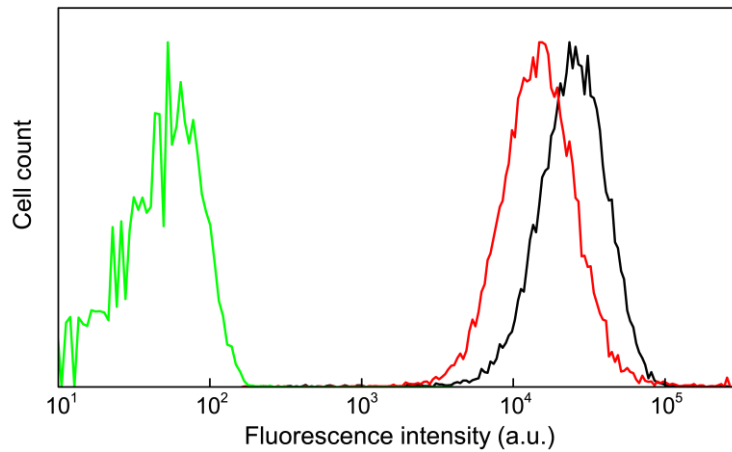


Fig. S10. Expression of CD44 on untreated and M β CD-treated KG1a cells was determined by flow cytometry. Untreated control (black) and M β CD-treated (red) KG1a cells were labelled with CD44 antibodies followed by AF-488-conjugated secondary antibodies. The green lines show the result on unstained KG1a cells. The data confirmed that the M β CD treatments did not affect the expression of CD44 molecules on the KG1a cells.

Supplementary Note. Depth of the field in the super-resolution localization microscopy imaging experiments with HILO configuration

The thickness of the beam with our HILO configuration (NA of the objective = 1.49, illumination area = 10 – 15 μm in diameter) is estimated to be approximately 6 μm . Therefore, we detected the fluorescence spots of single AF-647 dyes located at different positions along the axial axis in the 2D super-resolution localization microscopy imaging experiments.

However, we filtered out the localizations whose spot size (i.e., standard deviation of the 2D Gaussian function used for the fitting of the spots) was larger than 200 nm during the reconstruction of the super-resolution images. The threshold corresponds to the axial range of approximately ± 500 nm (fig. S11). Thus, the effective depth of the field in the 2D super-resolution images obtained in this study is approximately 1 μm , which is much larger than that in the quantitative dynamic footprinting method (up to 200 nm).

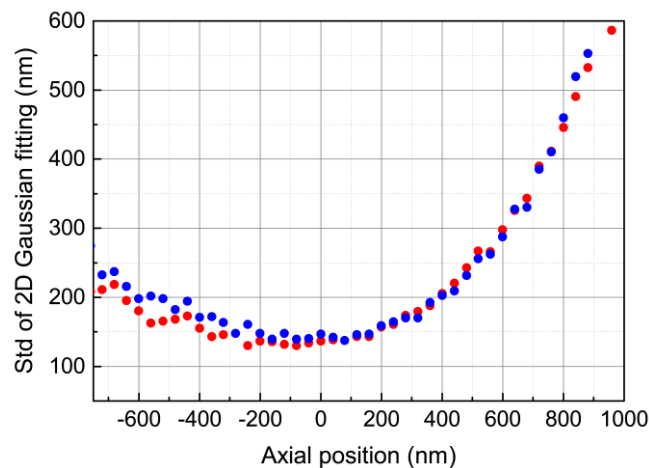


Fig. S11. Depth of the field in the SR localization microscopy imaging experiments with HILO configuration. Standard deviations of the 2D Gaussian function along X (red) and Y (blue) axis used for fitting the fluorescent spots obtained from TetraSpeck fluorescent microspheres (Invitrogen) deposited on a clean coverslip. The images were recorded at the axial positions between -700 and 1000 nm upon excitation at 638 nm.

Captions for Supplementary Video

Movie S1. Time-lapse transmitted light microscopy images of KG1a cells perfused into the microfluidic chamber at the shear stress of $0.25 \text{ dyne cm}^{-2}$. The surfaced of the chamber was coated by recombinant E-selectins at the density of $3.6 \text{ molecules } \mu\text{m}^{-2}$. Scale bar = $100 \mu\text{m}$.

Movie S2. Time-lapse transmitted light microscopy images of KG1a cells perfused into the microfluidic chamber at the shear stress of 0.5 dyne cm^{-2} . The surfaced of the chamber was coated by recombinant E-selectins at the density of $3.6 \text{ molecules } \mu\text{m}^{-2}$. Scale bar = $100 \mu\text{m}$.

Movie S3. Time-lapse transmitted light microscopy images of KG1a cells perfused into the microfluidic chamber at the shear stress of 1.0 dyne cm^{-2} . The surfaced of the chamber was coated by recombinant E-selectins at the density of $3.6 \text{ molecules } \mu\text{m}^{-2}$. Scale bar = $100 \mu\text{m}$.

Movie S4. Time-lapse transmitted light microscopy images of KG1a cells perfused into the microfluidic chamber at the shear stress of 2.0 dyne cm^{-2} . The surfaced of the chamber was coated by recombinant E-selectins at the density of $3.6 \text{ molecules } \mu\text{m}^{-2}$. Scale bar = $100 \mu\text{m}$.

Movie S5. Time-lapse transmitted light microscopy images of KG1a cells perfused into the microfluidic chamber at the shear stress of 4.0 dyne cm^{-2} . The surfaced of the chamber was coated by recombinant E-selectins at the density of $3.6 \text{ molecules } \mu\text{m}^{-2}$. Scale bar = $100 \mu\text{m}$.

Movie S6. Time-lapse transmitted light microscopy images of KG1a cells perfused into the microfluidic chamber in the presence of EDTA (10 mM) at the shear stress of 1.0

dyne cm⁻². The surfaced of the chamber was coated by recombinant E-selectins at the density of 3.6 molecules μm^{-2} . Scale bar = 100 μm .

Movie S7. Time-lapse transmitted light microscopy images of KG1a cells perfused into the microfluidic chamber at the shear stress of 1.0 dyne cm⁻². The surfaced of the chamber was coated by recombinant E-selectins at the density of 3.6 molecules μm^{-2} . Scale bar = 50 μm .

Movie S8. Time-lapse transmitted light microscopy images of M β CD-treated KG1a cells perfused into the microfluidic chamber at the shear stress of 1.0 dyne cm⁻². The surfaced of the chamber was coated by recombinant E-selectins at the density of 3.6 molecules μm^{-2} . Scale bar = 50 μm .